Geochemistry Geophysics Geosystems G3
AN ELECTRONIC JOURNAL OF THE EARTH SCIENCES
Published by AGU and the Geochemical Society

Article
Volume 10, Number 12
25 December 2009
Q12015, doi:10.1029/2009GC002881
ISSN: 1525-2027

Stagnant lid convection and the thermal subsidence of sedimentary basins with reference to Michigan

Norman H. Sleep
Department of Geophysics, Stanford University, Stanford, California 94305, USA (norm@pangea.stanford.edu)

[1] The thermal subsidence of basins formed above thick continental lithosphere differs from that of young passive margin basins and of young oceanic crust in that stagnant lid convection supplies significant heat flow from the asthenosphere. The lithosphere eventually approaches thermal equilibrium where the convective heat added to its base balances the heat lost by conduction to the surface. This paper presents a simple parameterization that quantifies these effects for modeling basin subsidence. The convective heat flow scales with the current lithosphere thickness squared while the conductive heat flow scales inversely to current lithospheric thickness. The predicted thermal subsidence rate scales to the difference between the conductive and convective heat flows and wanes gradually over hundreds of millions of years. The formalism can be modified to represent thermal subsidence where plume material has ponded within a catchment of locally thinned lithosphere. The base of the plume material forms a stable stratification that suppresses convective heat flow from below while heat continues to conduct to the surface by conduction. The predicted initial thermal subsidence rate scales with the large difference between conductive and zero convective heat flow. It is thus much greater than beneath lithosphere underlain by ordinary asthenosphere for a given amount of total eventual thermal subsidence. The paper compares thermal subsidence predictions from the models with and without plumes with sedimentation data from the Michigan basin. Observed initial Late Cambrian through Lower Devonian sedimentation in the Michigan basin is rapid as expected from the plume model, but the Ordovician sedimentation rate is slower than before and after. It is conceivable that this irregularity in the sedimentation curve is associated with low eustatic sea level and sediment-starved conditions at the basin center in the Ordovician and Early Silurian periods, as opposed to irregular tectonics. Sedimentation poorly resolves a long tail of gradual subsidence that may extend to the present.

Components: 10,472 words, 5 figures.

Keywords: Michigan; mantle plumes; stagnant lid convection; hot spots; lithosphere.

Index Terms: 8169 Tectonophysics: Sedimentary basin processes; 8103 Tectonophysics: Continental cratons; 8137 Tectonophysics: Hotspots, large igneous provinces, and flood basalt volcanism.

Received 25 September 2009; **Revised** 26 October 2009; **Accepted** 29 October 2009; **Published** 25 December 2009.

Sleep, N. H. (2009), Stagnant lid convection and the thermal subsidence of sedimentary basins with reference to Michigan, *Geochem. Geophys. Geosyst.*, *10*, Q12015, doi:10.1029/2009GC002881.

1. Introduction

[2] The seafloor subsides as the aging oceanic lithosphere cools and contracts. In analogy, geophysicists recognized that thermal contraction of the lithosphere after a heating event is an attractive mechanism for the subsidence of passive margins and platform basins [*Sleep*, 1971; *Haxby et al.*, 1976; *Sleep and Snell*, 1976; *McKenzie*, 1978;

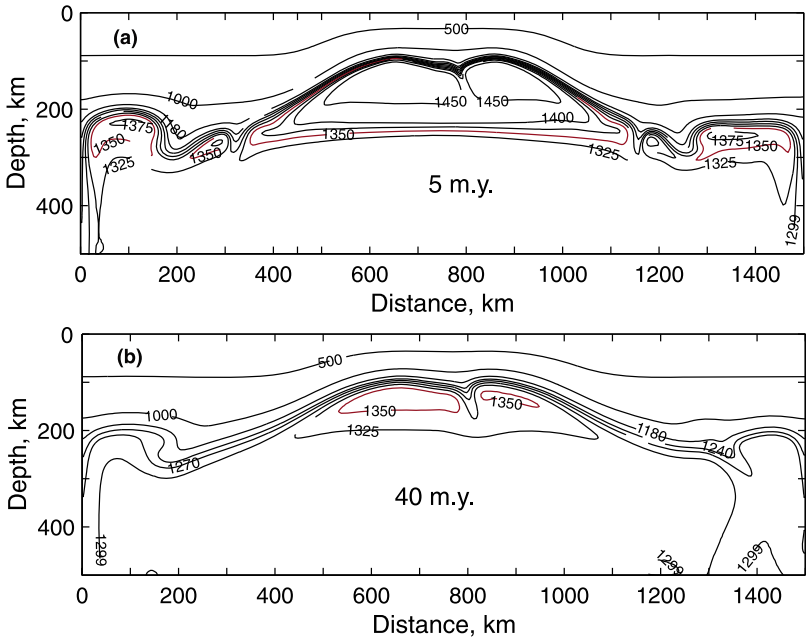

Figure 1. Computed isotherms in two dimensions at 5 Ma and 40 Ma after the impingement of a mantle plume serve as semischematic for the effect of plume material plumed beneath a catchment of thin lithosphere after *Sleep* [2003]. Convection transfers heat between hot plume material and the lithosphere, rapidly cooling the hottest plume material. Warm ponded plume material with sluggish convection persists for a long time. The base of the plume material is a stable buoyant interface that suppresses convective heat flow from the underlying mantle.

Nunn and Sleep, 1984; *Nunn et al.*, 1984; *Ahern and Dikeou*, 1989]. *Angevine et al.* [1990] and *Xie and Heller* [2009] in their reviews concluded that thermal contraction remains a viable mechanism for continental basin subsidence.

[3] Early thermal modelers used parameterized approaches out of necessity; full three-dimensional heat and mass transfer calculations were then unfeasible. Today, parameterization serves to illustrate basic scaling relationships and to provide quick predictions. Physically, heat leaves the lithosphere by conduction at the surface and enters the lithosphere by convection at its base. If the surface heat flow (minus that derived from radioactive heat generation) is more than the heat flow from below, the lithosphere cools and thickens. A steady state is eventually approached where the top and bottom heat flows match. Historically, modelers selected their boundary condition at the base of the lithosphere to allow approach to steady state, but with emphasis on numerical convenience. The classical "plate" model assumed that the base of the lithosphere at a given depth remained isothermal [*McKenzie*, 1967, 1978]. Constant heat flow at the base of the lithosphere is another simple boundary condition [e.g., *Kaminski and Jaupart*, 2000].

[4] The well-known formalism of stagnant lid convection provides means of quantifying the boundary condition at the base of this lithosphere in terms of physical parameters. In Appendix A, I algebraically manipulate well-known equations for heat flow to obtain calibrated dimensional expressions that do not involve rheological parameters. I apply these equations in section 2. I emphasize the difference of subsidence in the aftermath of pure lithospheric stretching from the aftermath of ponding of plume material beneath a local closed region of thin lithosphere. A convecting rheological boundary layer continues to supply heat to stretched lithosphere. In contrast, the base of ponded plume material is a stable buoyant interface so that convection from below provides no heat flow (Figure 1). As shown in section 2, the net effect is that the initial thermal subsidence of a basin above trapped plume material is much more rapid than the initial thermal subsidence above stretched lithosphere for a given amount of eventual thermal subsidence.

[5] The Michigan basin provides a real-world example with which to compare subsidence predictions with sedimentation observations (Figure 2). It accumulated a few kilometers of near sea level sediments during the Paleozoic Era. This process

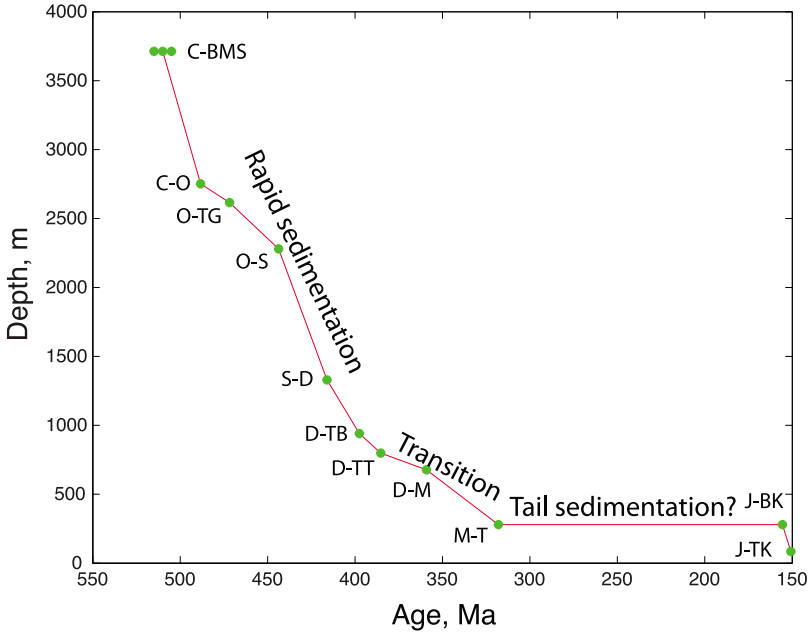

Figure 2. Depth-age curve for sediments in the McClure Sparks 1–8 borehole. There is a well-resolved period of rapid sedimentation transitioning into a poorly resolved tail of slow sedimentation. The sedimentation rate is slower in the Ordovician than immediately before or after that period. Horizons are as follows: C-BMS, Cambrian base of Mount Simon, ±5 Ma error bars are given for reference; C-O, Cambrian Ordovician boundary; O-TG, Ordovician, top Glenwood; O-S, Ordovician-Silurian boundary; S-D, Silurian-Devonian boundary; D-TB, Devonian top Bell Shale; D-TT, Devonian top Traverse; D-M, Devonian-Mississippi; M-T, top Mississippian; J-BK, Jurassic bottom of Kimeridgian; and J-TK, Jurassic top of Kimeridgian. Note that Pennsylvanian sediments occur over much of the center of the Michigan basin but not at this borehole; for reference the end of the Pennsylvanian is 299 Ma. Depths after *Hinze et al.* [1978]. Ages from International Commission on Stratigraphy Chart (http://www.stratigraphy.org/column.php?id=Chart/Time%20Scale, cited 25 June 2009).

represents differential vertical tectonics between the center of the basin and the surrounding arches that are now 350–400 m above sea level [e.g., *Hagadorn et al.*, 2002]. I present computed models in section 3 and discuss the detailed situation in Michigan in section 4. Note that "Michigan" here refers to the area of the Michigan basin centered in its Lower Peninsula for brevity unless otherwise stated. It includes parts of Indiana, Ohio, Ontario, the Upper Peninsula, and Wisconsin. I concentrate on this basin as it appears to be only weakly affected by later events. The Hudson Bay basin is similar but the tail of the sedimentation curve has been eroded and subsidence begins in the Late Ordovician, not late Cambrian [*Hanne et al.*, 2004]. Unlike Michigan, there is evidence for stretching of the lithosphere before subsidence. My models do not include the direct effect of lithospheric stretching on subsidence as the geological record in Michigan precludes significant stretching after 503 Ma. See section 4.4.

[6] I acknowledge that highly sophisticated calculations of basin subsidence associated with phase changes have been applied to Michigan [*Hamdani et al.*, 1991; *Naimark and Ismail-Zadeh*, 1995]. *Schoofs et al.* [2000] modeled subsidence associated with hydrothermal circulation in the basement. These mechanisms are beyond the scope of this paper to maintain simplicity.

2. Scaling Relationships for Basin Subsidence

[7] My objective is to obtain expression for subsidence associated with changes in lithospheric temperature. I use the geotherm in a hypothetical region with steady state as a reference toward which heated lithosphere evolves to provide scaling and clarify terminology (Figure 3). The temperature at the free surface is 0°C for simplicity. The geotherm approaches the mantle adiabat at the base of the lithosphere. A thin (5–20 km) region of the upper crust has significant radioactivity. Both conduction and convection occur within the rheological boundary layer at the base of the lithosphere. The

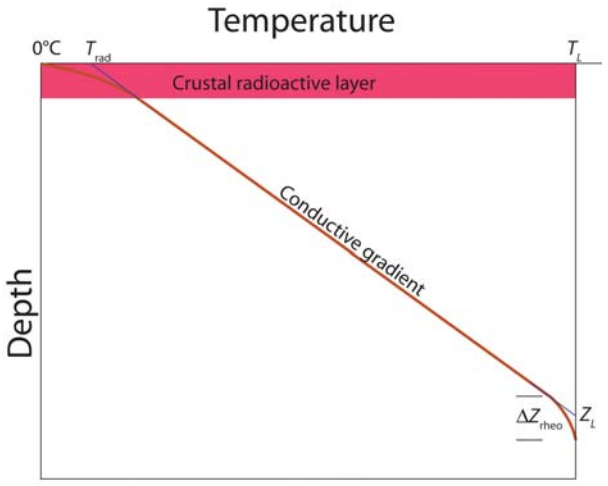

Figure 3. Schematic diagram of steady state geotherm through continental lithosphere. For simplicity the thermal conductivity is assumed to be constant. The geothermal gradient decreases with depth within the radioactive area of the upper crust. It decreases from the conductive gradient to the adiabatic gradient within the rheological boundary layer at the base of the lithosphere. The conductive gradient extrapolates to the temperature $T_{\rm rad}$ at the free surface and to the scale thickness of the lithosphere Z_L at the mantle adiabat T_L. The thickness of the rheological boundary layer is $\Delta Z_{\rm rheo}$. Rapid uniform stretching of the lithosphere (the pure shear model of *McKenzie* [1978]) leaves the shape of the geotherm unchanged by reducing the depth to any given temperature by a constant factor.

mantle below the rheological boundary layer is adiabatic.

2.1. Kinematic Relationship Between Subsidence and Heat per Area

[8] The steady state value thickness of the lithosphere Z_{ss} in equilibrium with stagnant lid convection is a convenient parameter for beginning the analysis. I obtain considerable simplification by assuming that the thermal gradient is linear throughout the lithosphere before steady state is reached. That is, I ignore the difference between $T_{\rm rad}$ and 0°C, the curvature of the geotherm associated with transient cooling, and the difference between the actual geotherm in the rheological boundary layer and the linear extrapolation (Figure 3). See Appendix A for discussion. Two parameters, the instantaneous scale thickness Z_L and the mantle abiabat T_L then define a linear geotherm

$$T = z\frac{T_L}{Z_L}, \tag{1}$$

where z is depth. I presume for now that the temperature of the mantle abiabat below Z_L is constant at T_L and that the thickness of the lithosphere evolves with time.

[9] I next present the well-known relationships between heat flow and subsidence. The heat deficit per area in the lithosphere relative to a reference at the mantle adiabat is

$$H = \int_0^{Z_X} \rho C(T_L - T)dz = \frac{\rho C Z_L T_L}{2}, \tag{2}$$

where ρC is volume specific heat (density times specific heat per mass), H and Z_L are functions of time, and the final equality uses the approximate temperature distribution in (1). The upper limit (maximum depth) of the integral needs to be taken so $Z_X > Z_L$. Similarly, the tectonic subsidence relative to the reference mantle adiabat (beneath air) is

$$S = \int_0^{Z_X} \alpha(T_L - T)dz = \frac{\alpha Z_L T_L}{2}, \tag{3}$$

where α is the volume thermal expansion coefficient.

[10] Continuing with forethought to obtain an expression for subsidence rate, the rate of decrease in heat per area within a column is the time derivative of (2) (again ignoring radioactivity) is the difference between the top and the bottom heat flows

$$q_{\rm top} - q_{\rm bot} = \frac{\partial H}{\partial t} = \frac{\rho C T_L}{2}\frac{\partial Z_L}{\partial t}, \tag{4}$$

Combining equations (3) and (4), the tectonic subsidence rate is

$$\frac{\partial S}{\partial t} = \left[\frac{\alpha}{\rho C}\right](q_{\rm top} - q_{\rm bot}) = \frac{\alpha T_L}{2}\frac{\partial Z_L}{\partial t}. \tag{5}$$

This expression implies that we need to know the surface and basal heat flows to predict subsidence but not the detailed temperature within the lithosphere. It applies when the thermal expansion coefficient and the volume heat capacity are relatively constant. This assumption is grossly inapplicable for phase changes such as basalt to eclogite modeled by *Hamdani et al.* [1991] and *Naimark and Ismail-Zadeh* [1995]. My treatment thus applies only to ordinary thermal contraction.

2.2. Top and Basal Heat Flow

[11] It is necessary to evaluate the top and basal heat flow to apply (5). I obtain expressions in terms of the heat per area H and the subsidence relative to the adiabat S. See Appendix A for discussion of the errors associated with this method and application to young oceanic lithosphere. The heat flow from conduction from (1) is simply

$$q_{\text{top}} = \frac{kT_L}{Z_L} = \frac{k\rho C T_L^2}{2H}. \tag{6}$$

As shown in Appendix A, the heat flow at the base of the lithosphere from stagnant lid convection is proportional to the lithospheric thickness squared Z_L^2. It is thus also proportional to H^2. For purposes of this paper, the approach to steady state is relevant. A calibrated expression for this basal heat flow near steady state is thus

$$q_{\text{bot}} = q_{ss}\left[\frac{H}{H_{ss}}\right]^2, \tag{7}$$

where the eventual steady state heat per area $q_{ss} = q_{\text{bot}} = q_{\text{top}}$ is

$$H_{ss} = \frac{k\rho C T_L^2}{2q_{ss}}. \tag{8}$$

This expression includes the volume specific heat ρC, which is reasonably constrained, the thermal gradient q_{ss}/k, and the mantle adiabat temperature T_L. The thermal gradient measured from the xenolith geotherm in stable platform regions [e.g., *Bell et al.*, 2003; *Francis and Patterson*, 2009] provides a reasonable proxy for the steady state thermal gradient. The rounded value 1350°C for T_L is used in recent treatments of the xenolith geotherm [e.g., *Francis and Patterson*, 2009]. One does not need to know rheological parameters, only the form of (7) and that steady state is eventually approached.

[12] Equation (4) then becomes

$$\frac{\partial H}{\partial t} = \frac{k\rho C T_L^2}{2}\left[\frac{1}{H} - \frac{H^2}{H_{ss}^3}\right]. \tag{9}$$

This equation has the practical advantage that the heat deficit per area H is the time-dependent variable that one needs to obtain subsidence history. The right hand side contains expressions for the top and bottom heat flows in terms of H. Equation (6) is the specific relationship used to obtain heat flow from heat deficit per area and is correct as a dimensional relationship where the computed result differs slightly from the result that would be obtained by an exact calculation. The requirement for approach to steady state in (7) calibrates the second term in (9) in terms of the first term. The first-order effect of the approximations thus can be represented in the calibrated form of (9) by multiplying the right hand side by a dimensionless constant that slightly differs from 1. The net effect is that of not knowing the physical constants, the mantle heat flow in (8), and the mantle adiabatic temperature precisely. These errors associated with the approximations implicit in (9) are discussed in Appendix A.

[13] The relationship in terms of subsidence using (9) is

$$\frac{\partial S}{\partial t} = \frac{\kappa\alpha^2 T_L^2}{2}\left[\frac{1}{S} - \frac{S^2}{S_{ss}^3}\right], \tag{10}$$

where $\kappa \equiv k/\rho C$ is the thermal diffusivity. Equation (8) calibrates this expression. Note that one obtains the constant basal heat flow analog of (9) and (10) by setting $H = H_{ss}$ and $S = S_{ss}$ in the final term in the bracket.

2.3. Subsidence Beneath Ponded Plume Material

[14] It is geometrically possible for a closed region of thin lithosphere to exist in a continental interior. This region may from a catchment for ponded plume material (Figure 1). This situation cannot exist along a passive margin of a significant ocean basin.

[15] Modification of (9) and (10) for this situation is straightforward. The large effect is that the basal heat flow is zero. As shown in Appendix A, the expression (6) for conductive heat flow q_{top} is a reasonable approximation. Stagnant lid convection continues beneath stable reference regions, which remain near steady state.

[16] The main conceptual difficulty is that the plume material eventually cools to the mantle adiabat and thereafter stagnant lid convection becomes established beneath the lithosphere. The timing for these processes depends on the thickness of the initial plume material and the detailed physics of convection. I modify (9) and implicitly (10) to formally represent this situation

$$\frac{\partial H}{\partial t} = \frac{k\rho C T_L^2}{2}\left[\frac{1}{H} - F(t)\frac{H^2}{H_{ss}^3}\right]. \tag{11}$$

The function $F(t) = 0$ when plume material is present and is 1 when stagnant lid convection is established. It transitions between these values

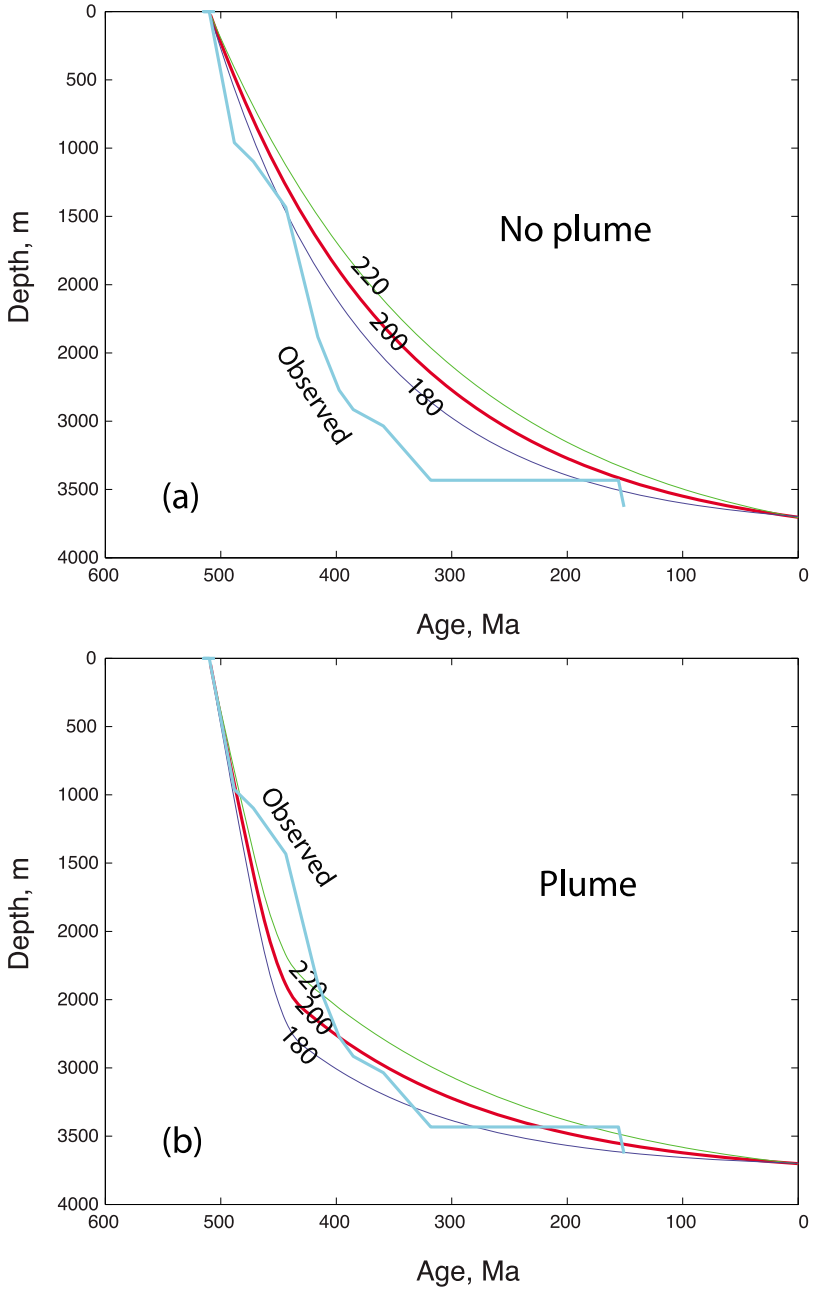

Figure 4. Computed models for sedimentation in the Michigan basin for various steady state lithosphere thicknesses. (a) The computed curves with no plume lie systematically above the observed curve. (b) The plume model curves pass through the observed curve but do not fit the irregularities in the curve.

once plume material has cooled to the mantle adiabat. I use a linear transition with time in the calculations for convenience.

3. Subsidence Models for the Michigan Basin

[17] I discuss the Michigan basin as a real example to illustrate the implications of subsidence beneath thinned lithosphere and subsidence beneath plume material. The thickness of sediments obtained from boreholes provides an estimate of tectonic subsidence *S*. Several assumptions are necessary to calibrate numerical models using (9), (10), and (11) to this situation.

[18] First, various units within the Michigan basin consist of rocks deposited near sea level. Correlated units deposited at highstands exist on the flanks

of the basins. Samples from outliers, kimberlite pipes, sinkholes, and meteor craters indicate that thin veneers of highstand sediments covered much of the adjacent craton at various times including the Ordovician through Upper Devonian Periods [e.g., *Velbel*, 2009]; sediments last covered the craton in the Mesozoic Era [*Patchett et al.*, 2004]. Late Cambrian shallow marine sediments exist on the west basin flank in central Wisconsin [*Hagadorn et al.*, 2002]. The difference in elevation of units on the flanks with those near the center of the basin thus provides a measure of the net amount of differential subsidence. I thus use the flanks as a proxy for a region where the lithosphere has remained near steady state. The top of the borehole in Figure 2, 232 m elevation [e.g., *Hinze et al.*, 1978], is modestly lower than the flank elevations of Cambrian in central Wisconsin 350–400 m [*Hagadorn et al.*, 2002]. For convenience, I calibrate subsidence curves to pass through the current top of the borehole and the basement-sediment contact. Specifically, I assume that the total sedimentation was 3700 m starting from the time of the oldest rocks 510 Ma to present. This uniquely defines the solution of (10) for given physical constants, mantle adiabat, and mantle heat flow in (8). Note that the maximum thickness of sediments in the basin is ~4800 m [*Fisher et al.*, 1988].

[19] It is necessary to adjust the computed subsidence rate for the load of the sediments. One way is to back strip and correct for the load, the paleowater depth, and eustatic sea level [*Watts and Ryan*, 1976; *Steckler and Watts*, 1978]. *Hinze et al.* [1978] measured the density of Michigan basin sediments at the site in Figure 1 with a borehole gravity meter. Their average density ρ_{sed} is 2610 kg m^{-3} and does not vary significantly on the time and depth scales in Figure 1. I ignore sediment compaction on the grounds that the porosity of the Michigan basin sediments is overall minor [*Hinze et al.*, 1978] and that the compaction of these sediments occurred soon after their deposition. I thus did not perform back stripping, but rather compare computed subsidence rates with the sedimentation curve in Figure 1. Note that *Kominz et al.* [2001] back stripped the deepest boreholes in the Michigan basin. They state in their abstract that the tectonic subsidence shows a single cooling event beginning in the Cambrian and that the deviation of the sedimentation history from a smooth curve are associated with eustatic effects and water depth effects. I qualitatively interpret the irregularities in the sedimentation curve in section 4.1.

[20] I apply the first-order effect of point-wise isostasy to convert computed tectonic subsidence rates in computed predicted sedimentation rates:

$$S_{sed} = S\left[\frac{\rho_{man}}{\rho_{man} - \rho_{sed}}\right], \tag{12}$$

where ρ_{man} is the density of the compensating layer in the mantle. *Fowler* [2005, p. 292–293] derives this expression for oceanic crust where water (not sediment fills) the depression. Application to sedimentary basins ignores that fact the uppermost basement heats up when sediments bury it [see *Kominz*, 1995]. In the case of Michigan, the effect is small as the sediment section has hard rock thermal conductivities [*Speece et al.*, 1985] and because the sediment thickness is much less than the lithosphere thickness. Equation (12) should not be used for thick low-conductivity sediments on young oceanic crust. The density of the compensating mantle is ~3400 kg m^{-3} in the calculations. By assumption, the temperature and density of this asthenospheric compensating region remain constant. Section A7 discusses how to include the secular cooling of the deep interior of the Earth in the models.

3.1. Computed Subsidence Models

[21] I computed subsidence models of predicted sedimentation rate by explicitly integrating (9) and (11). The relevant physical parameters are reasonably constrained. I use that the thermal conductivity is 3 W m^{-1} K^{-1}, the thermal expansion coefficient is 3×10^{-5} K^{-1}, and the volume specific heat is 4 MJ m^{-3} K^{-1}. The temperature of the base of the lithosphere is 1350°C.

[22] Xenolith geotherm studies provide estimates steady state scale thickness of the lithosphere or equivalently the heat flow within stable lithosphere. I vary these parameters to show their effects because they are not precisely constrained. I let the steady state lithospheric thickness vary from 180 to 220 km implying heat flows from 22.5 to 18.4 mW m^{-2}, which are reasonable [e.g., *Kaminski and Jaupart*, 2000]. I use 200 km for quick example calculations.

[23] Figure 4a shows models for thinned lithosphere and Figure 4b shows models for lithosphere above ponded plume material. The models include only thermal contraction and not the effect of lithospheric extension, which could cause very

rapid subsidence. As discussed in section 4.4, the geological record precludes significant lithospheric extension beneath Michigan after 503 Ma. The thinned lithosphere model predicts gradual sedimentation with initial rates somewhat slower than observed. The plume curve predicts initial rapid sedimentation as the basal heat flow is initially zero. The factor $F(t)$ in (11) is somewhat a free parameter. With Figure 1 in mind, I let it be 0 for the first 40 Ma and with forethought I let it increase linearly to 1 in the next 40 Ma and let it be 1 thereafter.

[24] The steady state lithospheric thickness has a minor affect on the results. Assuming an initial thickness below minimum assumed value of 180 km would improve the fit to the initial period of rapid sedimentation of the thinned lithosphere models in Figure 4a but would be inconsistent with xenolith geotherms. Increasing the steady state thickness would degrade with fit for these models.

3.2. Scaling Calculations

[25] I present simple scaling calculations to aid in the understanding of the computed models. First, the models were calibrated to give a total subsidence of 3700 m. The computed change in lithospheric thickness to obtain this quantity is independent of the scale thickness of the lithosphere Z_L:

$$S_{\mathrm{sed}} = \left[\frac{\rho_{\mathrm{man}}}{\rho_{\mathrm{man}} - \rho_{\mathrm{sed}}}\right]\left[\frac{\alpha \Delta Z_L T_L}{2}\right]. \qquad (13)$$

This expression for the assumed parameters yields that the lithosphere changes thickness by 42.5 km. This change is <1/4 of the assumed final steady state thicknesses. The assumption in (9), (11), and in Appendix A that the lithospheric thickness is modestly less than the steady state thickness is thus justified.

[26] With regard to plume material, the initial thickness of ponded material Z_P with an excess temperature of ΔT_P that provides a given amount of total sediment accumulation is

$$S_{\mathrm{sed}} = \left[\frac{\rho_{\mathrm{man}}}{\rho_{\mathrm{man}} - \rho_{\mathrm{sed}}}\right]\alpha Z_P \Delta T_P, \qquad (14)$$

Assuming an initial excess temperature of 250 K yields a thickness of 115 km which cannot be geometrically trapped by lithosphere that is ~50 km thinner than its surroundings. Rather, a lesser thickness to plume material becomes trapped within a closed region of previously thinned lithosphere as in Figure 1. It is conceivable that a plume tail could gradually resupply plume material to a lithospheric catchment allowing in to gradually thin the lithosphere. The effect that ponded plume material suppresses convection from the underlying mantle is important here. I do not attempt to resolve a thickness of ponded plume material and the initial lithospheric thinning as there are not data to do this.

[27] It is also straightforward to estimate the imbalance between surface conductive heat flow and basal conductive heat flow. I use an initial ~110 Ma interval of ~3000 m of sedimentation to provide a stable numerical example. The predicted heat flow imbalance is

$$\Delta q = \frac{\partial S_{\mathrm{sed}}}{\partial t}\left[\frac{\rho_{\mathrm{man}}}{\rho_{\mathrm{man}} - \rho_{\mathrm{sed}}}\right]^{-1}\left[\frac{\rho C}{\alpha}\right], \qquad (15)$$

which is 26.8 mW m^{-2} for the parameters used above. The equivalent scale thickness for the lithosphere for this heat flow is 151 km.

4. Discussion Relevant to Michigan

[28] The subsidence model including the aftermath of a mantle plume in Figure 4b does not provide a precise fit to observed sedimentation. Still the difference between this model and one without a plume in Figure 4a is illustrative. That is, the plume model predicts initial rapid sedimentation followed by transition to a tail of slow sedimentation. There is a strong hint of tail sedimentation in the data (Figure 2).

[29] It is convenient to discuss topics out of chronological order. I begin with the slow sedimentation in the Ordovician Period, then continue with tail sedimentation, and finish with information on the initial timing of subsidence and information on lithospheric stretching and plume events.

4.1. Slow Ordovician Sedimentation

[30] It is unclear from the sedimentation curve (Figure 2) whether there are separate Cambrian and Ordovician subsidence events. Earlier thermal models of the Michigan basin assumed two events and quantitatively considered the latter one: post-base Glenwood (Middle Ordovician and younger) subsidence. However, this interpretation depended on subsidence-time curves based on the absolute time scale then in use that had an excessive age for

the oldest Cambrian sediments in the basin. *Bond and Kominz* [1991] noted the issue of Cambrian and Ordovician absolute ages in Michigan. It is thus warranted to examine whether sedimentary effects caused slow Ordovician sedimentation; dynamically, whether subsidence began as a single event in the Cambrian and was thermally driven as concluded in an abstract by *Kominz et al.* [2001].

[31] For a quantitative model, one must adjust observed sedimentation for dynamic topography and true eustatic changes from variations in the volume of the ocean basins, as well as variations in water depth. In addition, sediments compact from the load of overlying sediments. In that case, compaction would reduce the present measured thickness to less than the deposited thickness and hence reduce measured sedimentation rate of the early sediments and increase the "tail" subsidence of later sediments.

[32] It is not now feasible to quantitatively separate eustasy from dynamic topography over a limited spatial region during the Paleozoic. Basically, both true eustasy and dynamic topography produce apparent sea level changes that vary little spatially on the scale of the Michigan basin. Neither can cause strong local subsidence of the center of the basin relative to its flanks. Importantly, the variations in the apparent rate of subsidence from a smooth curve correspond to similar variations in the western United States, as expected for thermal subsidence perturbed by sea level variations [*Kominz et al.*, 2001].

[33] Dynamic topography, however, may have resolvable effects as underlying slabs produce broad spatially varying subsidence. Passive margins surrounded North America at the start of the Cambrian subsidence. Active margins formed around the continent during the Paleozoic. There are currently passive margins, except on the west coast of North America. Current dynamic models include the effect of the Farallon slab [*Moucha et al.*, 2008; *Spasojevic et al.*, 2009]. Dynamic topography from the Ordovician slab to the east may have tilted the basin [*Howell and van der Pluijm*, 1999].

[34] I specifically discuss slow Ordovician sedimentation to point out the differences between a closed interior basin and a passive margin. During times of sea level regression, sedimentation may cease on exposed land producing a hiatus. Previously, deposited sediments may erode producing a degradational vacuity [e.g., *Wheeler*, 1963]. A productive assumption is to assume that tectonic (here thermal) subsidence continued during the missing interval.

[35] In general, variations into the water depth during deposition tend to have the systematic effect of reducing the current thickness of early sedimentary units at the center of the basin and increasing the thickness of later sediments. That is, the center of a basin may initially subside too rapidly to be filled with sediments. Once the subsidence rate has waned, later sediments are likely to fill the starved depression.

[36] A key difference which passive margins in this regard is that marine sedimentation ceased within the Michigan basin whenever sea level regressed below a sill on its flanks. The center of the basin could well have subsided below the paleo–sea level and remained dry land in the arid climate. The Ordovician prebase Glenwood (strictly prebase Saint Peter Sandstone) interval of slow net sedimentation includes the great continent-wide unconformity between the Sauk and Tippecanoe sequences of *Sloss* [1963]. Continental glaciation and hence low eustatic sea level continued into at least the Early Silurian [e.g., *Cocks and Rong*, 2008]. Silurian evaporite deposits eventually filled the starved center of the Michigan Basin [*LoDuca*, 2009]. Thus qualitatively, the Ordovician and Silurian deviations of Michigan sedimentation from a smooth curve can be attributed to eustatic and facies effects.

4.2. Tail Sedimentation

[37] Observed sedimentation is a poor recorder of slow tectonic subsidence. In the case of Michigan, Late Mississippian, Pennsylvanian, and Jurassic sediments marginally resolve tail subsidence. Marine conditions persisted episodically until the early Pennsylvanian, but subsequent sediments are nonmarine and hence do not provide good relative subsidence information [*LoDuca*, 2009]. Still, the areal extent of these units corresponds to the concentric "bull's eye" pattern of the underlying thick units and points to a shared tectonic cause. Compaction of older basin sediments cannot be confidently excluded as a mechanism as it too would be most active near the center of the basin.

[38] In particular, fission track and organic maturity studies indicate that a thick wedge of (low thermal conductivity, nonmarine) sediments buried the basin and surrounding Canadian Shield in the latest Pennsylvanian and Permian [*Crowley*, 1991; *Velbel*, 2009]. Deposition ceased when the orogen-

ic source to the east waned. By Jurassic time, erosion beveled the basin to a low-relief surface. Subsidence near the center of the basin by then had somewhat down dropped Pennsylvanian sediments thereby preserving the lowermost units. Nonmarine Jurassic deposits then accumulated in valleys incised into Pennsylvanian rocks under arid conditions and pollen studies indicate that these deposits were never deeply buried [*Velbel*, 2009]. Jurassic sediments may have in turn been systematically preserved near the center of the basin by slow subsidence after their deposition.

4.3. Timing of Start of Sedimentation in the Michigan Basin

[39] A key difference of Figure 2 from the sedimentation curve in the work of *Sleep and Sloss* [1978] is that a much younger absolute age is assigned to the deepest Cambrian deposits in the borehole. The absolute ages currently assigned to Cambrian stages are likely to be reliable and Figure 2 shows a ± 5 Ma error bar for reference, implying that this uncertainty does not affect the basic conclusions.

[40] However, the deep sediments in the Michigan basin are sparsely studied because of their inaccessibility and hence not well tied to the international absolute time scale. The deepest Paleozoic formation, the Mount Simon sandstone is effectively a catchall for the basal clastic sediments in this part of the Midwest. In Ohio, it lies on stream valleys and rifts associated with the breakup of the continent [*Reuter and Watts*, 2004]. Recent paleontological studies are not available for Michigan.

[41] The Mount Simon formation is thin at the borehole site so that one could start the subsidence analysis at its top, 3429 m depth, without affecting the conclusions. The overlying Eau Claire formation is dated in adjacent regions. Its oldest fossils are Dresbachian in age [*Palmer*, 1982; *Babcock*, 1994]. The age of the beginning of the equivalent international Guzhangian stage 503 Ma. The base of this formation provides a basin-wide paleo–near–sea level surface with which to measure relative subsidence. Significant stretching of the basin lithosphere after basal Eau Claire time would be obvious from the sedimentary record.

4.4. Mechanisms of Lithospheric Thinning and Crustal Loading

[42] For a basin to subside slowly by thermal contraction, the lithosphere needs to be heated above its steady state condition and the buoyancy of the lithosphere including the crust needs to be reduced below that of the crust (and lithosphere) that is at equilibrium sea level at steady state. Lithospheric stretching supplies both loading from thinning of the crust and the thermal event [*McKenzie*, 1978]. Subaerial erosion during a thermal uplift is a possible mechanism for thinning crust without stretching it [*Sleep*, 1971]. A broad domal uplift in the Cambrian at the current location of the Michigan basin in the Cambrian is implied by the erosion mechanism. As already mentioned, a combination of these processes is attractive as locally thinned lithosphere provides a catchment for plume material and hence a mechanism for doming. However, there is little evidence that a domal uplift shed sediments to surrounding regions.

[43] There is obviously Cambrian extension nearby related to the Iapetus and Ouachita breakup margins [see *Reuter and Watts*, 2004]. Plumes are also likely near young breakup margins. I review the dearth of data that bear on these issues. There is also no adjacent ocean basin to drive subsidence as at a passive margin [*Watts and Ryan*, 1976; *Steckler and Watts*, 1978].

[44] Note that *Angevine et al.* [1990] prefer the mechanism of *Haxby et al.* [1976] where igneous intrusions metamorphose the deep continental crust increasing its density. This process could well be associated with lithospheric stretching or plume activity, but there is no available data from Michigan that allows its appraisal.

[45] The Mount Simon sandstone provides sparse mostly negative information on loading mechanisms. It is not known to include rift faults or sediments within Michigan; the rift sediments and rift faults at the borehole site are Keweenawan ~1.1 Ga [*Van der Voo and Watts*, 1978; *Catacosinos*, 1981] and much too old to directly produce Cambrian thermal subsidence. However, the thickness of the Mount Simon is variable beneath Michigan. It is absent in southeastern Michigan, compatible with remnants of a domal uplift and thins to the northeastern margin of the basin [*Catacosinos*, 1973; *Catacosinos and Daniels*, 1991]. Provenance studies, however, might provide information on the detritus from accessible rocks on the basin flanks of the extent of pre–Mount Simon erosion. Irish Sea associated with the Iceland plume provides analogy; a radial system of drainage developed [*Cope*, 1994; *Sleep*, 2003]. This system of rivers, including the Thames, persists in the British Isles even though the

center of the uplift is beveled by erosion into a shallow sea.

[46] There is sparse evidence regarding thermal events in general. The nearest young volcanism penetrates basement rocks on the northeast flank of the basin [*Doig*, 1970]. The age of the Callander complex at the eastern end of Lake Nipissing, the nearest intrusion to Michigan, is ~577 Ma and the age of the Grenville dikes to the east is ~590 Ma [*Kamo et al.*, 1995]. There are ~4 m of undated barite-bearing sandstone that may be essentially synchronous with the nearby Manitou Islands intrusion [*Russell*, 1981]. The remaining marine sediments on islands within Lake Nipissing are much younger than the igneous activity, Middle to Late Ordovician ~475 Ma [*Ami*, 1899; *Russell*, 1981]. It is conceivable that they record reactivation of the local faults or a shallow arm of the sea that entered a river valley eroded into the weakened hard rocks of the rift.

[47] Keweenawan diabase at 5.32 km depth in the deep borehole in Figure 2 has been reset to a 500–700 Ma paleomagnetic pole, but the surrounding sediments have not been reset [*Van der Voo and Watts*, 1978]. *Ma et al.* [2009] interpret their noble gas data from deep brines in the Michigan basin as the product of fluid flow from the basement to the sedimentary column during fault reactivation at the end in the Mississippian [*Fisher et al.*, 1988]. These gas data do not bear on a possible Cambrian heating event.

[48] Xenolith geotherm data from kimberlites of different ages can resolve secular changes in the lithosphere [*Bell et al.*, 2003], but no suitable intrusions are known within the Michigan basin. *Griffin et al.* [2004] discussed kimberlites from the Upper Peninsula of Michigan on the northwest flank of the basin. These rocks are Middle Ordovician or younger ~475 Ma from fossil-bearing xenoliths. Unpublished radiometric ages are Jurassic [*Jarvis*, 1993], much too young for a Cambrian heating event. *Griffin et al.* [2004] suggest that mantle plumes emplaced lithosphere in this region on the basis of their petrology of mantle xenoliths.

5. Conclusions

[49] Calculations of thermal subsidence curves for continental interiors need to take explicit account of the heat balance in the lithosphere. Conduction causes heat to escape to the surface and stagnant lid convection supplies heat to its bottom. The predicted subsidence rate is proportional to the difference between these heat flows. It approaches zero as convection comes into balance with conduction so that the thermal structure of the lithosphere is in steady state.

[50] Models that predict the thermal subsidence history of basins conveniently represent stagnant lid convection with an effective boundary condition at the base of the lithosphere. Simple scaling equations (9) and (10) arise from the well-known formalism of parameterized convection where the convective heat flow is proportional to the current lithosphere thickness squared. The conductive heat flow is inversely proportional to current lithospheric thickness. The predicted approach of the lithosphere toward steady state is gradual over hundreds of millions of years.

[51] The formalism is easily modified to represent thermal subsidence associated with ponded plume material trapped in catchments of locally thin lithosphere. In that case, conduction continues to vent heat to the surface. Stagnant lid convection ceases, as the base of the plume material is a stable buoyant stratification. The predicted initial thermal subsidence rate is rapid as it scales with the large difference between the conductive heat flow from surface and zero convective heat flow at base of the plume material.

[52] The Michigan basin provides a geological example. Overall, thermal subsidence associated with plume material trapped by thinned lithosphere is attractive. Sedimentation of the Michigan basin (Figure 2) then represents a single lithospheric cooling event beginning at ~510 Ma. This interpretation mandates that observed slow sedimentation in the Ordovician Period was associated with eustasy and starved conditions at the basin center. Thermal subsidence above plume material explains then the initial rapid sedimentation, ~3000 m in ~110 Ma. A tail of subsidence to the present is implied and marginally resolved by the sedimentation record.

[53] A Cambrian initiation of thermal subsidence is attractive because continental breakup occurred nearby at that time. Lithospheric stretching and mantle plumes are thus plausible heating mechanisms though not resolved within the basin itself.

Appendix A: Parameterized Lithospheric Thickness

[54] Equation (9) gives the surface conductive and bottom convective heat flows in terms of heat

deficit per area in a column. The surface heat flow term presumes the linear geothermal gradient in (1). This approximation ignores from top down: the effect of radioactive heat generation in the shallow continental crust, curvature of the geotherm associated with transient cooling of the lithosphere toward steady state, and the rheological boundary layer at the base of the lithosphere. It also assumes that the mantle adiabat does not change with time and the viscosity is linear. I begin by deriving the convective term, as it is needed to discuss errors associated with the conductive approximation. I conclude this with a discussion of three-dimensional models.

A1. Stagnant Lid Formalism

[55] I repeat the derivation for convective heat flow beneath a stagnant lid to dimensionally obtain the conductive term in (9) [*Sleep*, 2002, 2007; *Nyblade and Sleep*, 2003; *Sleep and Jellinek*, 2008]. I then use the requirement that the top and bottom heat flows approach steady state to calibrate heat flow expression and eliminate rheological parameters. The derivation seeks the laterally averaged convective heat flow associated with transient convection. The lithospheric and asthenospheric material has a strongly temperature-dependent viscosity. The rigid lithosphere forms a stagnant lid that does not convect (Figure 3). The underlying asthenosphere is essentially adiabatic. The rheological boundary layer occurs between those two regions. Its properties determine the vigor of convection.

[56] Empirically, the temperature range across the rheological boundary layer $\Delta T_{\rm rheo}$ scales as $\sim 2.4 T_\eta$ where T_η is the temperature needed to change viscosity by a factor of e [*Solomatov and Moresi*, 2000]. I dimensionally balance forces within the rheological boundary layer assuming the dimensional form of this relationship, $T_{\rm rheo} \approx T_\eta$. The thickness of the rheological boundary layer is $\Delta Z_{\rm rheo}$ is allowed to vary at this stage of the derivation. A hydrostatic assumption dimensionally yields the deviatoric stress within the boundary layer

$$\tau \approx \rho g \alpha T_\eta \Delta Z_{\rm rheo}, \tag{A1}$$

where g is the acceleration of gravity. The velocity within the boundary layer is dimensionally the product of the deviatoric stress τ and the thickness of the rheological layer divided by the viscosity of the asthenospheric material η

$$V \approx \frac{\rho g \alpha T_\eta \Delta Z_{\rm rheo}^2}{\eta}. \tag{A2}$$

The convective heat flow is the product of the volume heat capacity, the temperature contrast, and the velocity

$$q_{\rm bot} \approx \rho C T_\eta V \approx \frac{\rho C \rho g \alpha T_\eta^2 \Delta Z_{\rm rheo}^2}{\eta}. \tag{A3}$$

Making the assumption that the geotherm is well behaved, the thermal gradient in the rheological boundary layer scales with the conductive thermal gradient in the overlying lithosphere. Then the thickness of the thermal boundary layer dimensionally scales with the thickness of the lithosphere $T_L/Z_L \approx T_\eta/\Delta Z_{\rm rheo}$. This assumption applies, for example, if lithosphere is quickly mechanically thinned as in the work of *McKenzie* [1978]. Eliminating $\Delta Z_{\rm rheo}$ from (9) yields

$$q_{\rm bot} \approx \frac{\rho C \rho g \alpha T_\eta^4 Z_L^2}{\eta T_L^2}. \tag{A4}$$

The convective term in (9) is based on this expression. The calibrated form of (A4) used in (9) follows from (1) where $H \propto Z_L$. Hence $q_{\rm bot} \propto H^2$ at a given steady state H_{ss} yields (9) where rheological parameters have been eliminated.

[57] The approach to steady state provides a check on (A4), where one obtains the standard for stagnant lid heat flow. Then, $q_{\rm top} = q_{\rm bot} = kT_L/Z_L$ where the lithosphere has its steady state thickness Z_L/Z_{ss}. Solving for heat flow yields in (A4)

$$q_{ss} \approx \frac{kT_L}{Z_L} \approx 0.47 k T_\eta \left[\frac{\rho g_z \alpha T_\eta}{\kappa \eta}\right]^{1/3}, \tag{A5}$$

where $\kappa \equiv k/\rho C$ is thermal diffusivity and the constant 0.47 was obtained by *Davaille and Jaupart* [1993a, 1993b, 1994] from laboratory experiments where the material properties were known.

A2. Effects of Radioactive Heat Generation

[58] Equation (1) ignores the effect of shallow radioactive heat generation on the geotherm. I ignore variations of thermal conductivity for simplicity as the sediments in the basin and the underlying Keweenawan sediments have high thermal conductivities comparable hard crustal and mantle rocks [*Speece et al.*, 1985]. The surface heat flow is the sum of the heat flow from the mantle and the total heat flow generated by radioactivity $q_{\rm sur} = q_{\rm top} + q_{\rm rad}$, where

$$q_{\rm rad} = \int_0^{z_b} A \quad dz, \tag{A6}$$

where there is no significant radioactive heat generation below depth z_b and A is radioactive heat generation per volume, a function of depth. The heat flow as a function of depth is

$$q = q_{\text{top}} + \int_z^{z_b} A \quad ds \tag{A7}$$

where s is a dummy variable for depth. The temperature in the lithosphere below depth z_b follows a linear gradient

$$T = T_{\text{rad}} + \frac{z q_{\text{top}}}{k} \tag{A8}$$

where the temperature at depth extrapolates to T_{rad} at the surface (Figure 3). The temperature at depth z_b calibrates this relationship:

$$T_b = \int_0^{z_b} \frac{q}{k} dz = \frac{z_b q_{\text{top}}}{k} + \frac{1}{k} \int_0^{z_b} dz \int_z^{z_b} A \quad ds, \tag{A9}$$

where the final right hand term is T_{rad}. Integrating by parts yields a more easily visualized expression,

$$T_{\text{rad}} = \frac{1}{k} \int_0^{z_b} zA \quad dz = \frac{q_{\text{rad}} Z_{\text{rad}}}{k} \tag{A10}$$

where

$$Z_{\text{rad}} = \left(\int_0^{z_b} zA \quad dz \right) \div \left(\int_0^{z_b} A \quad dz \right) \tag{A11}$$

is the mean depth of the radioactive heat generation.

[59] *Speece et al.* [1985] present heat flow data for the Michigan basin. Their presentation method provides input only for a generic example. Typical current heat flow is ~50 mW m^{-2} so q_{rad} is ~30 mW m^{-2} for a reasonable of q_{top}, ~20 mW m^{-2}. The average depth of heat generation in Michigan is unknown as Keweenawan sediments often bury unexposed crustal granites including those at the borehole site. I use the relatively large depth Z_{rad} of 10 km for an example to obtain T_{rad} = 100°C. This value is still small compared to the temperature at the base of the lithosphere ~1350°C. My models ignored the difference between T_{rad} and O°C.

A3. Effect of the Basal Thermal Boundary Layer

[60] Equations (1), (2), and (9) ignore the difference between the actual temperature distribution in the rheological boundary layer and the linear thermal gradient extrapolated from the rigid lithosphere (Figure 3). A simple model by *Sleep and Jellinek* [2008] for the rheological boundary layer suffices to show that this effect is quite small. They assumed that the laterally averaged conductive heat flow decreases linearly with depth in the rheological boundary layer

$$q = q_{\text{bot}} \left[\frac{z_B - s}{z_B} \right], \tag{A12}$$

where q_{bot} is the conductive heat flow through the stagnant lid and s is the depth below the top of the rheological boundary layer, and the depth scale

$$z_B = \frac{2ka_1 T_\eta}{q_{\text{bot}}}, \tag{A13}$$

where the dimensionless constant $a_1 \approx 2.4$ [*Solomatov and Moresi*, 2000]. Evaluating (2) heats the heat per area deficit

$$H \approx \frac{\rho C k}{q_{\text{bot}}} \left[\frac{T_L^2}{2} + \frac{a_1^2 T_\eta^2}{6} \right]. \tag{A14}$$

The first term in the bracket is the term obtained in (2) assuming a linear thermal gradient. The second term is the effect of the thermal boundary layer. The ratio of these terms $a_1^2 T_\eta^2 / 3 T_L^2$ provides the relative error from ignoring the thermal boundary layer. For example, T_η = 60 K implies an error of 0.4%.

A4. Conductive Heat Loss Above Plume

[61] Equation (11) assumes that the relation between heat flow with heat deficit per area in (2) applies approximately to lithosphere above ponded plume material. I present a graphical method in Figure A1 to show this assumption is reasonable.

[62] The area of the green triangle is equal to the red triangle ABC representing the excess heat of the plume material.

[63] The linear conductive gradient for thin lithosphere with an equivalent amount of heat in the column is also similar (Figure A1). Quantitatively, the area of the green triangle 0-Z_L-A is equal to that of the red triangle ABC representing the excess heat of the plume material,

$$\frac{1}{2}(Z_A - Z_L) T_L = \frac{1}{2}(Z_C - Z_A)(T_P - T_L), \tag{A15}$$

where Z_A and Z_C are the depths of these points and T_P T_P is the maximum temperature of the plume

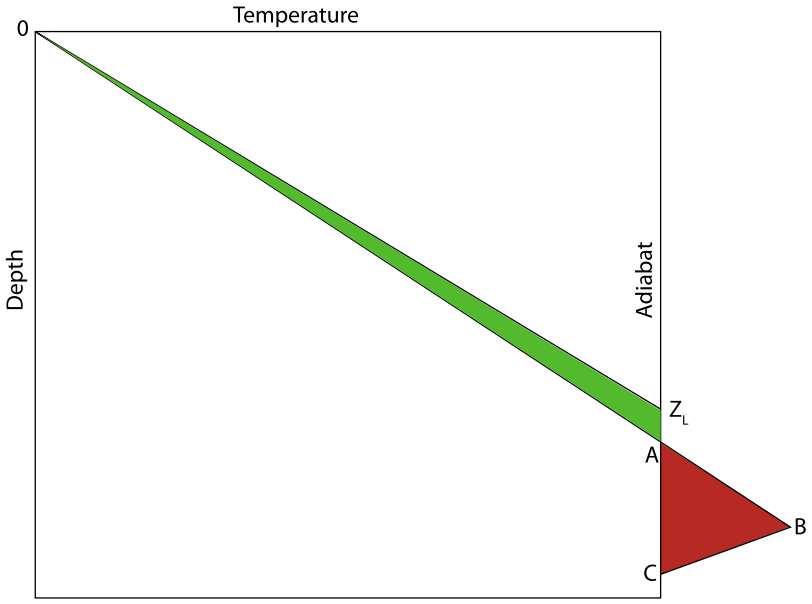

Figure A1. Schematic diagram shows the effect of representing heat deficit per area to obtain heat flow. The geotherm without plume material 0-Z_L has the same deficit as plume geotherm 0-ABC. The area of the green triangle is equal to the red triangle ABC representing the excess heat of the plume material.

material. The relative error in using Z_L to represent conductive heat flow is

$$\frac{Z_A - Z_L}{Z_L} = \frac{(Z_C - Z_A)(T_P - T_L)}{Z_L T_L}. \tag{A16}$$

For an example calculation, I assume a 100 km thick layer of plume material with a maximum excess temperature of 250 K. I let Z_L be 150 km and retain T_L at 1350°C. The relative error is 12%.

[64] In the Earth, the hottest plume material persists only briefly as viscosity is strongly temperature-dependent and the vigor of convection in (A4) depends on viscosity. The initial convection thins the lithosphere leaving a sluggishly convecting layer of somewhat warm plume beneath thinned lithosphere (Figure 1). This situation persists for a long time, over 40 Ma in Figure 1.

A5. Transient Cooling of the Lithosphere and Application to Oceanic Crust

[65] The linear geotherm (1) used to obtain heat flow q_{top} as a function of heat deficit per area H in (9) is an approximation, since transient cooling of the lithosphere implies a curved geotherm. The cooling of oceanic crust by conduction provides an upper estimate of the error in (9) associated this effect. The temperature of a half-space initially at T_L is

$$T = T_L \text{erf}\left(z/\sqrt{4\kappa t}\right), \tag{A17}$$

where t is plate age. The heat flow is

$$q_{\text{top}} = \frac{kT_L}{\sqrt{\pi\kappa t}}, \tag{A18}$$

and the heat deficit per area is

$$H = \rho C T_L \sqrt{\frac{4\kappa t}{\pi}}, \tag{A19}$$

all from *Fowler* [2005, chapter 7.5]. Combining (A18) and (A18), (6) and (9) with conduction only becomes

$$\frac{\partial H}{\partial t} = \frac{2k\rho C T_L^2}{\pi}\left[\frac{1}{H}\right]. \tag{A20}$$

The heat flow predicted by (A20) for a given value of H is a factor of $4/\pi = 1.27$ times that in (6) and (9), but the form of the leading term remains the same. Overall the form of (9) obtained by replacing the leading factor of (9) with the leading factor in (A20) is attractive for modeling oceanic lithosphere where $H \ll H_{ss}$, while (9) itself is attractive

for continental interiors where the lithospheric thickness is modestly less than the steady state value. The former limit requires some calibration as the heat deficit per area versus time curve extrapolates to a value H_{ss} that is not exactly the actual limit reached at long times.

A6. Approach to Steady State

[66] It is illustrative to manipulate (9) so its final approach to steady state can be compared with analytic equations using other boundary conditions. Using making the bracket in (9) dimensionless and bringing H_{ss} into the derivative yields

$$\frac{\partial(H-H_{ss})}{\partial t} = \frac{k\rho C T_L^2}{2H_{ss}}\left[\frac{H_{ss}}{H} - \frac{H^2}{H_{ss}^2}\right] = -\frac{k\rho C T_L^2}{2H_{ss}^2}(H-H_{ss})\left[\frac{H}{H_{ss}} + 1 + \frac{H_{ss}}{H}\right]. \quad \text{(A21)}$$

This term in the final bracket is >3 and approximately 3 for values of H/H_{ss} relevant to Michigan. For example, $H/H_{ss} = 3/4$ yields 3.08 for this term. Thus (A21) behaves like a decaying exponential with a time constant of

$$t_{ss} = \frac{2H_{ss}^2}{3k\rho C T_L^2} = \frac{k\rho C T_L^2}{6q_{ss}^2}. \quad \text{(A22)}$$

This expression has the general property that the time to approach steady state scales with the time for the final lithosphere thickness to come into conductive equilibrium [*Choblet and Sotin*, 2000]. For example, the condition of constant basal heat flow used by *Kaminski and Jaupart* [2000] is obtained by setting the final term in the bracket of the second expression in (A21) to 1. The factor 1/6 = 0.167 in (A22) then becomes 1/2. That is, constant bottom heat flow implies a slow approach to steady state. This time scale for a plate model with given basal temperature at depth Z_{ss} is $1/\pi^2$ = 0.101 [*McKenzie*, 1967, 1978; *Fowler*, 2005, p. 242]; it is $4/\pi^2$ = 0.405 for a plate model with given heat flow at a given depth Z_{ss} (obtained by from unnumbered equation following (7.74) of *Fowler* [2005] by replacing her L (my Z_{ss}) with $2L$ in her Fourier $n = 1$ term so that $\partial T/\partial z = 0$ at $z = L$).

A7. Secular Cooling of the Adiabatic Mantle

[67] The interior of the Earth has cooled over its history so that the thermal structure of the lithosphere cannot reach precise equilibrium. Current estimates are that the temperature of the mantle adiabat has decreased over the last 3 Ga by ~50 K Ga^{-1} [*Abbott et al.*, 1994; *Galer and Mezger*, 1998]. Stagnant lid convection has thus become less vigorous beneath younger "platform" lithosphere with the composition of ordinary mantle, including that beneath Michigan, over time. There has thus been a tendency for platforms to subside relative to cratons underlain by more ancient chemically buoyant lithosphere that remains at constant thickness [*Sleep*, 2005; *Sleep and Jellinek*, 2008]. Cratonic basement thus preferentially outcrops relative to platform basement. This process does not explain the differential subsidence of central Michigan relative to surrounding platforms.

[68] The effect can be included in (9) with the requirement that the steady state heat flow in (8) depends on the viscosity of the asthenosphere in (A5). The change of the reference adiabat with time in the lithosphere produces a virtual heat source (or heat flow) from (2),

$$\frac{\partial H}{\partial t} = \int_0^{Z_X} \rho C \frac{\partial T_L}{\partial t} dz = \frac{2H}{T_L}\frac{\partial T_L}{\partial t}, \quad \text{(A23)}$$

that is added to the right hand side of (9). Assuming 200 km thick lithosphere, the previously used physical parameters, and a cooling rate of 50 K Ga^{-1} yields a equivalent heat flow of 1.27 mW m^{-2}, which is within the uncertainty of the actual mantle heat flow. This term needs to be included (9) for both the reference stable site and the basin site to compute relative subsidence in a calculation that retains this effect.

A8. Caveat on Nonlinear Rheology

[69] The parameterized equations in section A1 assume a linear rheology. As a caveat, I point out that the subsidence history predicted by a nonlinear rheology differs significantly from that predicted by a linear rheology.

[70] My nonlinear approach follows *Solomatov and Moresi* [2000] and *Choblet and Sotin* [2000]. I briefly present the results in the notation of *Sleep* [2007]. The transient heat flow analogous to (A3) is dimensionally

$$q_N = \frac{\rho C T_\eta \left(\rho g \alpha T_\eta Z_{\text{rheo}}\right)^N Z_{\text{rheo}}}{\eta_H \tau_{\text{ref}}^{N-1}}, \quad \text{(A24)}$$

where the strain rate is $\tau^N/(\tau_{\text{ref}}^{N-1}\eta_H)$, τ_{ref} is a reference stress, and η_H is the viscosity of the

underlying half-space at that stress. Equation (9) then becomes

$$\frac{\partial H}{\partial t} = \frac{k\rho C T_L^2}{2}\left[\frac{1}{H} - \frac{H^{N+1}}{H_{ss}^{N+2}}\right]. \quad \text{(A25)}$$

The case where $N = 3$ provides an example. The lithosphere was thinned to ~3/4 of its steady state value in the models. In a linear $N = 1$ model, the initial convective term was 56% of its final value. It is 31% of its final value in the nonlinear case. That is, nonlinear rheology produces initial rapid subsidence as in the plume model in Figure 4b.

A9. Parameterized Three-Dimensional Models

[71] It is relatively easy to extend the dimensional parameterization in (9) to treat basin wide subsidence with such lateral heat conduction. Qualitatively, lateral conduction of heat acts as a lateral averaging filter on thermal subsidence and hence does not change the basin-wide amount of subsidence. The region above the hot center of the thermal anomaly cools faster than it would in one dimension and the surrounding cooler regions cool more slowly [*Kaminski and Jaupart*, 2000]. They used a narrow thermal anomaly within the lithosphere to obtain initial rapid subsidence near the center of the basin as shown in Figure 2.

[72] Mathematically, the heat flow equation for constant thermal conductivity is

$$\rho C\frac{\partial T}{\partial t} = k\left[\frac{\partial^2 T}{\partial x^2} + \frac{\partial^2 T}{\partial y^2} + \frac{\partial^2 T}{\partial z^2}\right], \quad \text{(A26)}$$

where x and y are horizontal coordinates. Integrating with depth using (2) yields

$$\frac{\partial H}{\partial t} = \kappa\left[\frac{\partial^2 H}{\partial x^2} + \frac{\partial^2 H}{\partial y^2}\right] + q_{\text{top}} - q_{\text{bot}}. \quad \text{(A27)}$$

A coarse horizontal numerical grid suffices as parameterized convection predicts only a laterally average heat flow and as conduction quickly removes short wavelengths. Flexure then can be included in a straightforward manner along with realistic sediment loads and compaction. *Angevine et al.* [1990] review how to this in practice.

Acknowledgments

[73] This research was in part supported by NSF grants EAR-0406658 and EAR-0909319. The latter grant is funded under the American Recovery and Reinvestment Act of 2009 (ARRA) (Public Law 111–5). I became aware of the existence of the Michigan basin and the need to find an explanation for its subsidence during undergraduate classes taught by James Fisher and William Hinze at Michigan State University in the 1960s. The Hudson Bay workshop at the Spring 2009 AGU meeting renewed my interest in the topic. Michelle Kominz provided comments on an earlier version of the paper and two helpful reviews. An anonymous reviewer provided many detailed helpful comments. Larry Heaman quickly responded to my questions on the absolute ages of igneous intrusions on the flanks of the Michigan Basin.

References

Abbott, D. L., L. Burgess, J. Longhi, and W. H. F. Smith (1994), An empirical thermal history of the Earth's upper mantle, *J. Geophys. Res.*, *99*, 13,835–13,850, doi:10.1029/94JB00112.

Ahern, J. L., and P. J. Dikeou (1989), Evolution of the lithosphere beneath the Michigan Basin, *Earth Planet. Sci. Lett.*, *95*, 73–84, doi:10.1016/0012-821X(89)90168-4.

Ami, H. M. (1899), On some Cambro-Silurian and Silurian fossils from Lake Temiskaming, Lake Nipissing, and Mattawa outliers, *Geol. Surv. Can. Annu. Rep.*, *10*(1), 289–302.

Angevine, C. L., P. L. Heller, and C. Paola (1990), *Quantitative Sedimentary Basin Modeling*, *Contin. Educ. Course Note Ser.*, vol. 32, 256 pp., American Association of Petroleum Geologists, Tulsa, Okla.

Babcock, L. E. (1994), Biostratigraphic significance and paleogeographic implications of Cambrian fossils from a deep core, Warren County, Ohio, *J. Paleontol.*, *68*(1), 24–30.

Bell, D. R., M. D. Schmitz, and P. E. Janney (2003), Mesozoic thermal evolution of the southern African mantle lithosphere, *Lithos*, *71*, 273–287, doi:10.1016/S0024-4937(03)00117-8.

Bond, G. C., and M. A. Kominz (1991), Disentangling middle Paleozoic sea level and tectonic events in cratonic margins and cratonic basins of North America, *J. Geophys. Res.*, *96*(B4), 6619–6639, doi:10.1029/90JB01432.

Catacosinos, P. A. (1973), Cambrian lithostratigraphy of Michigan basin, *Am. Assoc. Pet. Geol. Bull.*, *57*, 2404–2418.

Catacosinos, P. A. (1981), Origin and stratigraphic assessment of pre-Mt. Simon clastics of Michigan basin, *Am. Assoc. Pet. Geol. Bull.*, *65*, 1617–1620.

Catacosinos, P. A., and P. A. Daniels (1991), Stratigraphy of Middle Proterozoic to Middle Ordovician formations of the Michigan basin, in *Early Sedimentary Evolution of the Michigan Basin*, edited by P. A. Catacosinos and P. A. Daniels, *Spec. Pap. Geol. Soc. Am.*, *256*, 53–71.

Choblet, G., and C. Sotin (2000), 3D thermal convection with variable viscosity: Can transient cooling be described by a quasi-static scaling law?, *Phys. Earth Planet. Inter.*, *119*, 321–336, doi:10.1016/S0031-9201(00)00136-9.

Cocks, L. R. M., and J. Rong (2008), Earliest Silurian faunal survival and recovery after the end Ordovician glaciation: Evidence from the brachiopods, *Earth Environ. Sci. Trans. R. Soc. Edinburgh*, *98*, 291–301.

Cope, J. C. W. (1994), A latest Cretaceous hotspot and the southeasterly tilt of Britain, *J. Geol. Soc.*, *151*, 905–908, doi:10.1144/gsjgs.151.6.0905.

Crowley, K. D. (1991), Thermal history of Michigan basin and southern Canadian Shield from apatite fission-track analysis, *J. Geophys. Res.*, *96*, 687–711.

Davaille, A., and C. Jaupart (1993a), Thermal convection in lava lakes, *Geophys. Res. Lett.*, *20*, 1827–1830, doi:10.1029/93GL02008.

Davaille, A., and C. Jaupart (1993b), Transient high-Rayleigh-number thermal convection with large viscosity variations, *J. Fluid Mech.*, *253*, 141–166, doi:10.1017/S0022112093001740.

Davaille, A., and C. Jaupart (1994), The onset of thermal convection in fluids with temperature-dependent viscosity: Application to the oceanic mantle, *J. Geophys. Res.*, *99*, 19,853–19,866, doi:10.1029/94JB01405.

Doig, R. (1970), An alkaline rock province linking Europe and North America, *Can. J. Earth Sci.*, *7*, 22–28.

Fisher, J. H., M. W. Barratt, J. B. Droste, and R. H. Shaver (1988), Michigan Basin, in *The Geology of North America, vol. D-2, Sedimentary Cover—North America Craton*, edited by L. L. Sloss, pp. 361–382, Geol. Soc. of Am., Boulder, Colo.

Fowler, C. M. R. (2005), *The Solid Earth: An Introduction to Global Geophysics*, 2nd ed., 685 pp., Cambridge Univ. Press, Cambridge, U. K.

Francis, D., and M. Patterson (2009), Kimberlites and aillikites as probes of the continental lithospheric mantle, *Lithos*, *109*, 72–80, doi:10.1016/j.lithos.2008.05.007.

Galer, S. J. G., and K. Mezger (1998), Metamorphism denudation and sea level in the Archean and cooling of the Earth, *Precambrian Res.*, *92*, 389–412, doi:10.1016/S0301-9268(98)00083-7.

Griffin, W. L., S. Y. O'Reilly, B. J. Doyle, N. J. Pearson, H. Coopersmith, K. Kivi, V. Malkovets, and N. Pokhilenko (2004), Lithosphere mapping beneath the North American plate, *Lithos*, *77*, 873–922, doi:10.1016/j.lithos.2004.03.034.

Hagadorn, J. W., R. H. Dott, Jr., and D. Damrow (2002), Stranded on a Late Cambrian shoreline: Medusae from central Wisconsin, *Geology*, *30*(2), 147–150, doi:10.1130/0091-7613(2002)030<0147:SOALCS>2.0.CO;2.

Hamdani, Y., J. C. Mareschal, and J. Arkani-Hamed (1991), Phase-changes and thermal subsidence in intracontinental sedimentary basins, *Geophys. J. Int.*, *106*, 657–665, doi:10.1111/j.1365-246X.1991.tb06337.x.

Hanne, D., N. White, A. Butler, and S. Jones (2004), Vertical motions of Hudson Bay, *Can. J. Earth Sci.*, *41*, 1181–1200, doi:10.1139/e04-047.

Haxby, W. F., D. L. Turcotte, and J. M. Bird (1976), Thermal and mechanical evolution of Michigan basin, *Tectonophysics*, *36*, 57–75, doi:10.1016/0040-1951(76)90006-8.

Hinze, W. J., J. W. Bradley, and A. R. Brown (1978), Gravimeter survey in the Michigan deep borehole, *J. Geophys. Res.*, *83*, 5864–5868, doi:10.1029/JB083iB12p05864.

Howell, P. D., and B. A. van der Pluijm (1999), Structural sequences and styles of subsidence in the Michigan basin, *Geol. Soc. Am. Bull.*, *111*(7), 974–991, doi:10.1130/0016-7606(1999)111<0974:SSASOS>2.3.CO;2.

Jarvis, W. (1993), Michigan kimberlites: An update, in *Diamond Bearing Kimberlite and Related Geology in the Upper Peninsula of Michigan*, [CD-ROM], Mich. Basin Geol. Soc., Lansing.

Kaminski, E., and C. Jaupart (2000), Lithospheric structure beneath the Phanerozoic intracratonal basins of North America, *Earth Planet. Sci. Lett.*, *178*, 139–149, doi:10.1016/S0012-821X(00)00067-4.

Kamo, S. L., T. E. Krough, and P. S. Kumarapeli (1995), Age of the Grenville dyke swarm, Ontario-Quebec: Implications for the timing of Iapetan rifting, *Can. J. Earth Sci.*, *32*, 273–280, doi:10.1139/e95-022.

Kominz, M. (1995), Thermally subsiding basins and the insulating effect of sediment with application to the Cambro-Ordovician Great Basin sequence, western USA, *Basin Res.*, *7*, 221–233, doi:10.1111/j.1365-2117.1995.tb00107.x.

Kominz, M. A., D. Werkema, D. A. Barnes, W. Harrison III, E. Kirwan, and M. Malin (2001), The Michigan Basin is thermal in origin, *AAPG Bull.*, *85*, 1533–1534.

LoDuca, S. (2009), Paleozoic environments and life, in *Michigan Geology and Geography*, edited by R. Schaetzl, J. Darden, and D. Brandt, pp. 40–59, Custom, New York.

Ma, L., M. C. Castro, and C. M. Hall (2009), Crustal noble gases in deep brines as natural tracers of vertical transport processes in the Michigan Basin, *Geochem. Geophys. Geosyst.*, *10*, Q06001, doi:10.1029/2009GC002475.

McKenzie, D. P. (1967), Some remarks on heat flow and gravity anomalies, *J. Geophys. Res.*, *72*(24), 6261–6273.

McKenzie, D. (1978), Some remarks on development of sedimentary basins, *Earth Planet. Sci. Lett.*, *40*, 25–32, doi:10.1016/0012-821X(78)90071-7.

Moucha, R., A. M. Forte, J. X. Mitrovica, D. B. Rowley, S. Quéré, N. A. Simmonse, and S. P. Grand (2008), Dynamic topography and long-term sea-level variations: There is no such thing as a stable continental platform, *Earth Planet. Sci. Lett.*, *271*, 101–108, doi:10.1016/j.epsl.2008.03.056.

Naimark, B. M., and A. T. Ismail-Zadeh (1995), Numerical models of a subsidence mechanism in intracratonic basins: Application to North American basins, *Geophys. J. Int.*, *123*(1), 149–160, doi:10.1111/j.1365-246X.1995.tb06667.x.

Nunn, J. A., and N. H. Sleep (1984), Thermal contraction and flexure of intracratonal basins: A 3-dimensional study of the Michigan basin, *Geophys. J. R. Astron. Soc.*, *76*, 587–635.

Nunn, J. A., N. H. Sleep, and W. E. Moore (1984), Thermal subsidence and generation of hydrocarbons in the Michigan basin, *AAPG Bull.*, *68*, 296–315.

Nyblade, A. A., and N. H. Sleep (2003), Long lasting epeirogenic uplift from mantle plumes and the origin of the Southern African Plateau, *Geochem. Geophys. Geosyst.*, *4*(12), 1105, doi:10.1029/2003GC000573.

Palmer, A. R. (1982), Fossils of Dresbachian and Franconian (Cambrian) age from the subsurface of west-central Indiana, *Spec. Rep., 29*, 12 pp., Indiana Geol. Surv., Bloomington.

Patchett, P. J., A. F. Embry, G. M. Ross, B. Beauchamp, J. C. Harrison, U. Mayr, C. E. Isachsen, E. J. Rosenberg, and G. O. Spence (2004), Sedimentary cover of the Canadian Shield through Mesozoic time reflected by Nd isotopic and geochemical results for the Sverdrup Basin, Arctic Canada, *J. Geol.*, *112*, 39–57, doi:10.1086/379691.

Reuter, J., and D. R. Watts (2004), An ancient river channel system incised on the Precambrian–Cambrian unconformity beneath Jackson County, Ohio, *AAPG Bull.*, *88*(8), 1041–1047.

Russell, D. J. (1981), The geology of the Paleozoic outliers on the Canadian Shield, in *Summary of Field Work, 1981*, edited by J. Wood et al., *Misc. Pap.*, *100*, pp. 117–120, Ont. Geol. Surv., Toronto, Ont., Canada.

Schoofs, S., R. A. Trompert, and U. Hansen (2000), Thermochemical convection in and beneath intracratonic basins: Onset and effects, *J. Geophys. Res.*, *105*(B11), 25,567–25,585.

Sleep, N. H. (1971), Thermal effects of the formation of Atlantic continental margins by continental break-up, *Geophys. J. R. Astron. Soc.*, *24*, 325–350.

Sleep, N. H. (2002), Local lithospheric relief associated with fracture zones and ponded plume material, *Geochem. Geophys. Geosyst.*, *3*(12), 8506, doi:10.1029/2002GC000376.

Sleep, N. H. (2003), Fate of mantle plume material trapped within a lithospheric catchment with reference to Brazil, *Geochem. Geophys. Geosyst.*, *4*(7), 8509, doi:10.1029/2002GC000464.

Sleep, N. H. (2005), Evolution of continental lithosphere, *Annu. Rev. Earth Planet. Sci.*, *33*, 369–393, doi:10.1146/annurev.earth.33.092203.122643.

Sleep, N. H. (2007), Edge-modulated stagnant-lid convection and volcanic passive margins, *Geochem. Geophys. Geosyst.*, *8*, Q12004, doi:10.1029/2007GC001672.

Sleep, N. H., and A. M. Jellinek (2008), Scaling relationships for chemical lid convection with applications to cratonal lithosphere, *Geochem. Geophys. Geosyst.*, *9*, Q12025, doi:10.1029/2008GC002042.

Sleep, N. H., and L. L. Sloss (1978), A deep borehole in the Michigan basin, *J. Geophys. Res.*, *83*, 5815–5819, doi:10.1029/JB083iB12p05815.

Sleep, N. H., and N. S. Snell (1976), Thermal contraction and flexure of mid-continent and Atlantic marginal basins, *Geophys. J. R. Astron. Soc.*, *45*, 125–154.

Sloss, L. L. (1963), Sequences in the cratonic interior of North America, *Geol. Soc Am. Bull.*, *74*, 93–114, doi:10.1130/0016-7606(1963)74[93:SITCIO]2.0.CO;2.

Solomatov, V. S., and L.-N. Moresi (2000), Scaling of time-dependent stagnant lid convection: Application to small-scale convection on Earth and other terrestrial planets, *J. Geophys. Res.*, *105*, 21,795–21,817, doi:10.1029/2000JB900197.

Spasojevic, S., L. Liu, and M. Gurnis (2009), Adjoint models of mantle convection with seismic, plate motion, and stratigraphic constraints: North America since the Late Cretaceous, *Geochem. Geophys. Geosyst.*, *10*, Q05W02, doi:10.1029/2008GC002345.

Speece, M. A., T. D. Bowen, J. L. Folcik, and H. N. Pollack (1985), Analysis of temperatures in sedimentary basins: The Michigan Basin, *Geophysics*, *50*, 1318–1334, doi:10.1190/1.1442003.

Steckler, M. S., and A. B. Watts (1978), Subsidence of the Atlantic-type continental margin off New York, *Earth Planet. Sci. Lett.*, *41*, 1–13, doi:10.1016/0012-821X(78)90036-5.

Van der Voo, R., and D. R. Watts (1978), Paleomagnetic results from igneous and sedimentary rocks from the Michigan basin borehole, *J. Geophys. Res.*, *83*, 5844–5848, doi:10.1029/JB083iB12p05844.

Velbel, M. A. (2009), The "lost interval": Geology from the Permian to the Pliocene, in *Michigan Geology and Geography*, edited by R. Schaetzl, J. Darden, and D. Brandt, pp. 60–68, Custom, New York.

Watts, A. B., and W. B. F. Ryan (1976), Flexure of the lithosphere and continental margin basins, *Tectonophysics*, *36*, 25–44, doi:10.1016/0040-1951(76)90004-4.

Wheeler, H. E. (1963), Post-Sauk and pre-Absaroka Paleozoic stratigraphic patterns in North America, *Am. Assoc. Pet. Geol. Bull.*, *47*, 1497–1526.

Xie, X., and P. L. Heller (2009), Plate tectonics and basin subsidence history, *Geol. Soc. Am. Bull.*, *121*, 55–64.